Optimization of ion trajectories in a dynamically harmonized Fourier-Transform Ion Cyclotron Resonance cell using a Design of Experiments strategy

Julien Maillard, Justine Ferey, Christopher P. Rüger, Isabelle Schmitz-Afonso, Soumeya Bekri, Thomas Gautier, Nathalie Carrasco, Carlos Afonso, Abdellah Tebani

Optimization of ion trajectories in a dynamically harmonized Fourier-Transform Ion Cyclotron Resonance cell using a Design of Experiments strategy

Julien MAILLARD[1,2], Justine FEREY[2], Christopher P. Rüger[2], Isabelle SCHMITZ-AFONSO[2], Soumeya BEKRI[3], Thomas GAUTIER[1], Nathalie CARRASCO[1], Carlos AFONSO[2] and Abdellah TEBANI[2,3*]

[1] LATMOS/IPSL, Université Versailles St Quentin, UPMC Université Paris 06, CNRS, 11 blvd d'Alembert, F-78280 Guyancourt, France

[2] Université de Rouen, Laboratoire COBRA UMR 6014 & FR 3038, IRCOF, 1 Rue Tesnière, 76821 Mont St Aignan Cedex, France

[3] Department of Metabolic Biochemistry, Rouen University Hospital, Rouen, 76000, France

Abstract

The optimization of the ion trajectories in the ion cyclotron resonance (ICR) cell of a Fourier transform ICR mass spectrometer is a crucial step to obtain the best dynamic range, mass resolution, and mass accuracy. With the recent introduction of the dynamically harmonized cell, the complexity of tuning expanded drastically, and a fine-tuning of the DC voltages is required to optimize the ion cloud movement. This adjustment is typically performed manually.

Here, we propose a computational method based on a design of experiments (DoE) strategy to overcome the limits of classical manual tuning. This DoE strategy was exemplarily applied on a 12T FTICR equipped with a dynamically harmonized ICR cell. The chemometric approach, based on a composite central face design (CCF), was first applied on a reference material (sodium trifluoroacetate) allowing for the evaluation of the primary cell parameters. Eight factors were identified related to shimming and gating. The summed intensity of the signal corresponding to the even harmonics was defined as one quality criteria.

Consequently, the DoE response allowed for rapid and complete mapping of cell parameters resulting in an optimized parameter set. The new set of cell parameters was applied to the study of an ultra-complex sample. Here, Tholins, an ultra-complex mixture that mimics the haze present on Titan, was chosen. We observed a substantial improvement in mass spectrometric performance. The sum of signals related to harmonics was decreased by a factor of three (from 4% for conventional tuning to 1.3%). Furthermore, the dynamic range was also increased and lead to an increase of attributed peaks by 13%.

Graphical abstract

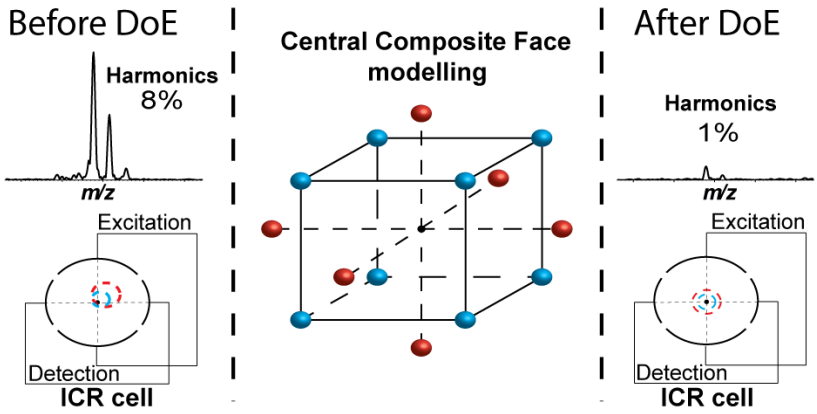

1. Introduction

Fourier Transform Ion Cyclotron Resonance mass spectrometer (FTICR) is well known to be the most powerful mass spectrometer by reaching unprecedented resolving power, mass accuracy and sensitivity levels[1,2]. It turned out to be the most appropriate instrument for the characterization of ultra-complex mixtures such as petroleum[3-7], natural organic matter [8] or extraterrestrial organic matter [9,10]. In order to detect the cyclotron motion, FTICR uses the combination of a static electric field which is hyperbolic near the center and a strong homogeneous static magnetic field (up to 21 Tesla – so far). The combination of both fields retains ions in the cell. Ions in the magnetic field travel according to a cyclotron motion defined by equation 1.

$$\omega_0 = \frac{qB_0}{m}$$

Equation 1: Cyclotron frequency (ω_0) of a charged particle in a homogeneous magnetic field. q is the charge of the particle, B_0 the strength of the magnetic field and m the mass of the particle.

In addition, the ion packet undergoes a drift of a trajectory equal to **ExB** where E is the electric field and B is the magnetic field. Both of these movements allow the ion packet to be trapped in the cell[2,11].

The shape of the ICR cell was improved steadily over time from first cubic geometry[12] to a variety of spherical designs varying in electrode shape and number [13]. As an example, the orthorhombic capacitively coupled cell developed by Steven Beu in 1991 [14] or the infinity cell which was designed by Caravatti et al. in 1991 are cited here [15], the later remaining the most commonly used nowadays . In recent instruments, the so-called dynamically harmonized cell is frequently deployed [2]. For the purpose of radiofrequency excitation and detection of ions, the cell is composed of several electrodes. In case of the dynamically

harmonized cell, these excitation and detection electrodes are specially shaped to compensate the quadrupolar electric field over the entire cell's body. It allows to produces a volume where, over the orbit of the ions, the average field is quadrupolar at all cyclotron radii. Thus, the frequency drifts of ions of the same mass over time along the Z axis are reduced. This makes possible to record transients for a longer time than in the previous cells and thus significantly improve performance

Optimized detection in terms of highest resolving power, sensitivity and dynamic range is obtained when the ion cloud is perfectly centered in the middle of the magnet. However, in practice, the imperfections of the alignment cause a bias in the position of the ion packets and thus a deviation in the cyclotron motion synchronization. This issue is solved by adding another set of segments to the dynamically harmonized cell in order to smooth imperfections by applying additional DC (Direct Current) voltages [11]. With this approach, it is possible to decrease the abundance of even-harmonic signals and, thus, to minimize magnetron motion. However, the values for the additionally applied DC voltages have to be tuned manually, which requires specially trained personnel and is tedious and time-consuming. In the present work, an experimental design approach is proposed in order to overcome the drawbacks of the manual ICR cell tuning. The approach seeks to optimize the DC voltages and reach the best set of parameters. Design of experiments (DoE) is a rigorous procedure in which defined modifications are induced based on a given set of variables. The response of the system is recovered to create a mathematical model, which allows a prediction of a set of parameters optimizing the response value[16-18]. Some example of mass spectrometer's optimization using DoE can be cite, such as the work performed by Lemonakis et al (2016) and Tebani et al (2016) [19,20]. Here, this method is applied on a defined response, the sum of the abundance of the second harmonic of sodium trifluoroacetate cluster.

After optimization, the obtained parameters are applied to the analysis of a complex mixture, Tholins. This synthetic material is used to understand the chemistry occurring in Titan's atmosphere by artificially mimicking the brown haze surrounding the largest moon of Saturn[21-25]. More importantly, Tholins have shown to be ultra-complex mixtures with high isobaric complexity and thousands of elemental compositions [26]. Tholins spectra obtained after DoE and after the usual manual method are compared. The potential of the developed method for complex mixtures analysis is highlighted evaluating the mass spectrometric performance, i.e., resolving power, the abundance of harmonics and number of detected signals.

2. Experimental methods

2.1. Tholins production

Tholins were produced following the PAMPRE procedure (French acronym for Aerosols Microgravity Production by Reactive Plasmas) presented elsewhere[24,27]. Briefly, in a stainless steel tubular reactor, a continuous gas mixture composed of 95 v-% nitrogen and 5 v-% methane was injected through polarized electrodes and evacuated by a primary vacuum pump system. A Radio Frequency – Capacity Coupled Plasma (RF-CCP) discharge was established in the gas mixture deploying an RF of 13.56 MHz. The pressure in the plasma discharge was maintained at 0.9 ± 0.1 mbar, and the reaction took place at room temperature (293 K).

2.2. Instrumentation

2.2.1. Fourier transform ion cyclotron resonance mass spectrometer

All analyses were performed on a FTICR Solarix XR from Bruker equipped with a 12T superconducting magnet and a dynamically harmonized ICR cell. The following ion transfer parameters were used for both electrospray (ESI) and laser desorption ionization (LDI) analyses in positive ion mode: capillary exit 150V, deflector plate 200V, funnel1 150V, skimmer1 25V, funnel RF amplitude 60Vpp, octopole frequency 5MHz, octopole RF amplitude 350Vpp, lower cut-off of the quadrupole at *m/*z 120, time-of-flight 0.7ms, frequency TOF 6MHz, TOF RF amplitude 200Vpp, side kick offset -1V, front and back trapping plate 1.75V.

For ESI the following parameters were used: capillary 4.5kV, spray shield -500V, dry gas flow 2L.min^{-1}, dry gas temperature 180°C, nebulizer gas flow 0.5bar. All analyses were recorded on 20 scans with a quadrupole accumulation time of 0.1s. Electrospray spectra

were recorded with a mass range from *m/z* 98 to 1,200 and a transient length of 2.2s. Sodium trifluoroacetate (NaTFA, Sigma Aldrich) at 0.1mg.ml^{-1} in ACN/H_2O (50/50, v/v) was used as a standard for the design of experiments approach.

Complex Tholins mixture analyses was recorded applying LDI. The solid sample was deposed on a MALDI plate following previous work[28]. The third harmonic of a Nd:YAG laser at 355nm delivering a maximum output of 0.5mJ (Smartbeam II, Bruker) was used to ionize the samples with the following parameters: laser power 15%, laser shots per scan 50, shots frequency 1kHz, plate offset 100V. The recorded mass spectra combined 800 scans to achieve high signal-to-noise. LDI spectra were recorded with a mass range from *m/z* 110 to 1200 and a transient length of 4.3s.

2.3. Experimental design

2.3.1. Software

DataAnalysis 4.4 (Bruker Daltonics GmbH, Bremen) was used to process all mass spectrometric analyses, including *m/z*-calibration and response recovering (abundance of the harmonic signals).

MODDE 11 software (Umetrics, Sartorius Stedim Data Analytics AB, Umea, Sweden) was used to perform the consecutive data analyses and modeling. The initial step is the definition of the response (i.e., user observation). Then, in a second step, factors influencing the response are defined. Afterward, several choices of experimental design shapes can be chosen. The software will automatically create the DoE given to the user as a coded matrix (**Table 1**) and a real matrix (**Table S1**). This matrix defines the experiments to be recorded and from which the response has to be extracted. Then, MODDE propose an automatic fitting method (e.g., partial least squares regression - PLS) allowing the visualization of the

quality and the predictability of the DoE. Finally, the optimizer tool was used to predict the set of parameters giving the best response result.

2.3.2. Factorial designs

The tuning of the ICR cell is established with eight principal parameters, four shimming parameters (shimming 0°, shimming 180°, shimming 90° and shimming 270°) and four gating settings (gated 0°, 90°, 180°, and 270°)[11]. The set of gating parameters represents the values of DC voltages applied during the injection in the ICR cell in order to correctly trap the ion packets. The set of shimming parameters represents the values of DC voltages applied for the excitation and the detection of the ions packets in the ICR cell. A simplified description of the ICR cell is given in **figure 1**. Other parameters of the ICR cell are not included (e.g., back and front plate voltages, sidekick offset) as they are easily and rapidly manually tunable. This significantly reduces the number of experiments required for the DoE approach, considerably decreasing the optimization time.

Parameters were grouped in pairs leading to four couples of parameters: shimming 0°-180° (Shi0), shimming 90°-270° (Shi90), gated 0°-180° (Gat0) and gated 90°-270° (Gat90) simplifying the optimization process compared to the conventional manual procedure. The values of these couples change symmetrically, meaning that when the value of one part is increased, the other part decreases about the same value. Initially, all values are set to 1.5V (default settings). As example, increasing the value of the shimming 0° about 50mV to 1.55V results at a value of the shimming 180° of 1.45V. In addition to these four coupled parameters, the sweep excitation power (SEP) was added as a factor parameter for the first step of the optimization strategy. SEP has a crucial impact on the ion trajectories as it defines their radius. After defining the assessed experimental factors, it was necessary to define the desired response as a result of the optimization. Following the classical

optimization method, the intensity ratio between the ion of the NaTFA at *m/z* 702.86324 and its second harmonic at *m/z* 351.43164 was recovered.

The optimization of the dynamically harmonized cell parameters was divided into two steps. The first screening step was performed with wide parameter intervals to evaluate the effects of each parameter on the defined response. The second part, named optimization experimental design, focused on narrower intervals to reach the best set of parameters. The applied chemometric approach for the two steps is based on a Composite Central Composite face design (CCF) which takes into account interactions between parameters. The coded CCF for the first step is given in **Table 1** formatted according to the required software input. Basically, the table reflects the conducted experimental plan, where -1 means that the parameter was set at the respective low level (e.g., for Shi 0 at 1.465V) and +1 at the respective high level. Defined intervals for each parameter are given in **Table 2** for the screening and optimization step. These intervals have been defined quickly by varying each of the parameters until the intensity of the harmonic reaches a minimum level. This step takes about 5 minutes.

2.3.3. Multivariate modeling

Partial Least Squares regression (PLS) was used to model each CCF design and to find the best set of parameters regarding the response chosen using the optimizer tool implemented in MODDE 11. Thus, PLS coefficients are used to estimate factor effects. A positive value of the coefficient indicates an increase of the response upon increasing the corresponding parameter, whereas a negative value indicates a decrease of the response upon increasing the corresponding parameter. The larger the absolute value of the PLS coefficient, the higher the effect of the parameter on the response. Analysis of variance (ANOVA) applied to the sum of squares of the PLS regression coefficient was used to assess the significance

of the factor effect. For a statistically significant effect of a factor, the model *p*-value of ANOVA should not exceed 0.05[29].

3. Results and discussion

3.1. Screening experimental design using NaTFA

The design of experiments approach was performed using NaTFA to minimize the abundance of signals related to harmonics. Briefly, the influence of four pairs of factors and the SEP (Shi0, Shi90, Gat0, Gat90, and Sweep Excitation Power) was evaluated using an even harmonic peak intensity of the ion *m/z* 702.86324 at *m/z* 351.43164 as the response. A Central Composite Face design (CCF) was chosen as it is generally applicable for this type of optimization problems.

Figure 2a visualizes the effect of the different factors on the even harmonic abundance in the screening step. SEP, Shi0, and Shi90 revealed the most significant effects on the intensity of the second harmonic peak, with contribution factors of 28.0%, 15.4%, and 33.3% respectively. SEP played a positive effect with high values leading to high abundance of the harmonic. In contrast, Shi0 and Shi90 showed a negative response, with high values resulting in low abundance of the harmonic. In addition, the interaction of Shi0 and Shi90 provided a significant positive effect, which is related to a high separation effect of these parameters. Hence these two couples of parameters have two very different effects on the abundance of the harmonic and, thus, on the ion cloud trajectories.

The prediction plot obtained based on the 27 experimental data points, between the predicted and observed values of the abundance of the second harmonic, is shown in **Fig. 2b**. This representation allows to access the quality of prediction with this model based on the initial data set. The cumulative modeled variation (R^2X = 99.1%) and the cumulative predicted variation (Q^2Y = 62.8%) reflect the explained variance and the predictability of

the model. The near to one R^2X value proves the validity of the model. The Q^2Y value (which is above 50%) proves that the model can give predictable values of parameters for the defined response [17,18,29]. However, this value could be improved to obtain better optimization results, which will be the aim of the following part of the optimization experimental design. The values of the regression coefficients and their respective *p*-values are given in **Table S-3** (Supplementary data). The fitted models' metrics, ANOVA and validation results of each model are presented in **Tables S-4** and **S-5** (Supplementary data).

Using this built model, the instrumental parameters were optimized to reach the lowest harmonic intensity. The predicted optimized values are presented in **Table 2.** Nevertheless, the obtained set of predicted values reach the extremity of each defined interval. Therefore, an additional optimization step was performed focusing on tight intervals for Shi0, Shi90, Gat0, and Gat90. It should be noted that the SEP and shimming values are two decorrelated parameters. In the rest of this study, the SEP was fixed at a value of 30% in order to focus on fine tuning. This value is a percentage of the maximum excitation amplitude.

3.2. Optimization experimental design using NaTFA

As described above, for this step, the sweep excitation power (SEP) was removed from the studied factors to focus only on the cell parameters. It turned out, that Shi0 and Shi90 had a major negative response on the second harmonic abundance (**Fig. 2c**), which is consistent with the results obtained in the previous screening step. Coded regression coefficients, ANOVA and model validation results are given in **Tables S-2, S-5, and S-6** (Supplementary data). The fitted model shows a cumulative modeled variation of R^2X = 99.5% and a cumulative predicted variation of Q^2Y = 88.9% as showed in **Fig. 2d**. These results improved compared to the screening step and proved the high predictability of the movement of ions in the dynamically harmonized cell. Using this built model, the

optimized set of parameters provided an abundance of 1.3% of second harmonics compared to the base signal. In comparison, the non-optimized parameters (manufacturer default values) provided 8% and manually optimized parameters provided 4% of harmonic abundance, respectively.

This first study proved the possible optimization of the movement of ions in the ICR cell by lowering harmonic peaks. This DoE methodology was validated by the study of a NaTFA standard solution typically used for instrument calibration and optimization. However, the high interest of optimizing the ion trajectories in the ICR cell is related to the description of complex mixtures with unknown constituents. Consequently, the set of parameters yielded by the DoE methodology have been applied to study Titan tholins. The results were compared to those obtained after the manual optimization.

3.3. Application for the analysis of complex mixtures: Titan tholins

The largest moon of Saturn, Titan, is surrounded by a thick and nitrogen-rich fog with some fraction of methane[30-33]. Understanding how this haze is produced along with its molecular composition are crucial steps from a planetary and prebiotic chemistry perspective[34,35]. Tholins are analogs of Titan's haze. They are laboratory-produced and used as a proxy on Earth as there is currently no sample return option. This material is an extremely complex mixture comparable to the complexity of petroleum and as such ideal for evaluating the tuning of the dynamically harmonized cell parameters[26]. **Figure 3** shows an overview of a tholins mass spectrum, containing more than 50,000 peaks. This mass spectrum was generated with LDI ionization together with the optimized cell tuning parameters resulting from the DoE approach on NaTFA. The insert in **Figure 3** presents the molecular complexity on a single nominal mass revealing more than 100 resolved peaks. In this study,

we used this ultra-complex sample to compare the effects of the above-described optimization strategy with the conventional method relying on manual optimization.

The comparison between the detected species applying the parameters given by manual tuning and DoE optimization is illustrated in **Figure 4**. The mass spectrum at the top was recorded after the conventional manual optimization of the ICR cell. This manual optimization can take several hours easily to obtain high performance due to the manual iteration process. The spectrum at the bottom was recorded after deploying the optimized parameter set given by the newly developed DoE strategy, which takes approximately one hour. It should be mentioned that the shimming parameters are re-optimized once a year to compensate instrumental's drift. Except for the cell parameters, the two spectra were recorded with the exact same conditions. The number of detected species is significantly higher with the DoE optimization. **Figure 4**, giving a small fraction of the mass spectrometric complexity revealed thirteen additional species (indicated with a red star) for the DoE optimized spectrum compared to the spectrum resulted after manual tuning. The attribution of these new peaks is given in **table S-7**. This observation can be induced by two effects: 1) The ion packets is more centered in the cell thanks to the computational method, inducing a higher dynamic range or, 2) in the spectrum after manual adjustment, some peaks are in coalescence with their close neighbor. This effect is not present after the DoE tuning, which explain why more peaks are observed in this case. In order to reinforce this, through attributions, it can be justified that these peaks are not harmonics. Manual optimization is a difficult and limited process. Indeed, it is impossible for the human eye to take into account the interactions between the various parameters.Therefore, the location of the ions is not perfectly centered and could still be improved. Furthermore, this method is a time-consuming iterative process based on trial and error steps to reach acceptable values specified by the manufacturer (here below 6% for the second harmonic). The above

described DoE strategy, performed with NaTFA, allows a complete mapping of the different parameter effects along with their interactions, which allows modeling of the system. Thus, this strategy leads to a more fine-tuning and a greater reduction of harmonics compared to the conventional manual attempt.

Different metrics obtained for DoE originated and manually recorded spectra are listed in **Table 3**. These results were obtained after recording 5 replicates for each tuning. As illustrated in **Figure 4** applying the DoE generated parameters significantly increased the number of observed peaks. The comparison with the manually tuned cell revealed 13% more peaks attributed after the DoE tuning. The resolving power is also slightly increased after the experimental design optimization: approx. 1,440,000 with the DoE method and 1,350 000 with the manual method at *m/z* 400. A slight increase is also observed for the average mass accuracy of the elemental composition assignment. All these results are summarized in **Figure 5**.

The application of the new predicted dynamically harmonized cell parameters on Titan's tholins showed a clear enhancement on almost every metric of the recorded spectrum in comparison with the spectrum generated with the non-tuned cell but also with the manually tuned cell. Furthermore, this work will be useful for the implementation of quadrupolar ion detection, which commonly induces higher order harmonics with increased abundance. This newly developed optimization strategy is highly time efficient compared to the conventional method, taking only one hour including the recording of the spectra, data processing, and data analysis.It is a universal approach and can be applied to any complex mixture such as petroleum and biological sample materials. Those ultra-complex mixtures usually raises high analytical challenges regarding experimental optimization.

4. Conclusions

The developed design of experiments (DoE) strategy has proven to be applicable for generating optimized parameter sets for a dynamically harmonized ICR cell. We could show that the approach results in settings leading to a reduction of harmonics to levels not reached by manual tuning and far below the manufacturer default values. Moreover, the optimization process takes significantly less time and can be performed by any instrument user. This substantial improvement allows for a better performance of the FTICR by significantly increasing all metrics of the recorded spectrum, i.e., mass accuracy, resolution and dynamic range, for both the standard as well as the ultra-complex mixture. Finally, this computational procedure based on a composite face design could be applied for any other mass spectrometric parameter optimization problem. The authors believe this will allow for a more transparent and more structured design when performing method development.

5. Acknowledgments

N.C. thanks the European Research Council for funding via the ERC PrimChem project (grant agreement No. 636829.).

Financial support from the National FT-ICR network (FR 3624 CNRS) for conducting the research is also gratefully acknowledged.

This work was also supported at COBRA laboratory by the European Regional Development Fund (ERDF N°31708), the Région Normandie, and the Labex SynOrg (ANR-11-LABX-0029) together with Normandie Université (NU), the Centre National de la Recherche Scientifique (CNRS), Université de Rouen Normandie (URN) and Innovation Chimie Carnot (I2C).

6. References

1. Smith RD, Cheng X, Bruce JE, Hofstadler SA, Anderson GA. TRAPPING, DETECTION AND REACTION OF VERY LARGE SINGLE MOLECULAR-IONS BY MASS-SPECTROMETRY. *Nature.* 1994;369(6476):137-139.
2. Nikolaev EN, Boldin IA, Jertz R, Baykut G. Initial experimental characterization of a new ultra-high resolution FTICR cell with dynamic harmonization. *Journal of the American Society for Mass Spectrometry.* 2011;22(7):1125-1133.
3. McKenna AM, Purcell JM, Rodgers RP, Marshall AG. Heavy Petroleum Composition. 1. Exhaustive Compositional Analysis of Athabasca Bitumen HVGO Distillates by Fourier Transform Ion Cyclotron Resonance Mass Spectrometry: A Definitive Test of the Boduszynski Model. *Energy & Fuels.* 2010;24(5):2929-2938.
4. Smith DF, Podgorski DC, Rodgers RP, Blakney GT, Hendrickson CL. 21 Tesla FT-ICR Mass Spectrometer for Ultrahigh-Resolution Analysis of Complex Organic Mixtures. *Analytical chemistry.* 2018;90(3):2041-2047.
5. Rodgers RP, McKenna AM. Petroleum analysis. *Analytical chemistry.* 2011;83(12):4665-4687.
6. Hughey CA, Rodgers RP, Marshall AG. Resolution of 11 000 Compositionally Distinct Components in a Single Electrospray Ionization Fourier Transform Ion Cyclotron Resonance Mass Spectrum of Crude Oil. *Analytical chemistry.* 2002;74.
7. Marshall AG, Rodgers RP. Petroleomics: chemistry of the underworld. *Proceedings of the National Academy of Sciences of the United States of America.* 2008;105(47):18090-18095.
8. Li L, Fang Z, He C, Shi Q. Separation and characterization of marine dissolved organic matter (DOM) by combination of Fe(OH)3 co-precipitation and solid phase extraction followed by ESI FT-ICR MS. *Analytical and bioanalytical chemistry.* 2019;411(10):2201-2208.
9. Schmitt-Kopplin P, Gabelica Z, Gougeon RD, et al. High molecular diversity of extraterrestrial organic matter in Murchison meteorite revealed 40 years after its fall. *Proceedings of the National Academy of Sciences of the United States of America.* 2010;107(7):2763-2768.
10. Schmitt-Kopplin P, Harir M, Kanawati B, Tziozis D, Hertkorn N, Gabelica Z. Chemical footprint of the solvent soluble extraterrestrial organic matter occluded in soltmany ordinary chondrite. *Meteorites.* 2012:79-92.
11. Jertz R, Friedrich J, Kriete C, Nikolaev EN, Baykut G. Tracking the Magnetron Motion in FT-ICR Mass Spectrometry. *Journal of the American Society for Mass Spectrometry.* 2015;26(8):1349-1366.
12. Guan S, Marshall AG. Ion traps for Fourier transform ion cyclotron resonance mass spectrometry: principles and design of geometric and electric configurations. *International Journal of Mass Spectrometry and Ion Processes.* 1995;146-147:261-296.
13. Marshall AG, Hendrickson CL, Jackson GS. Fourier transform ion cyclotron resonance mass spectrometry: A primer. *Mass Spectrometry Reviews.* 1998;17(1):1-35.
14. Beu SC, Laude DA. Open trapped ion cell geometries for Fourier transform ion cyclotron resonance mass spectrometry. *International Journal of Mass Spectrometry and Ion Processes.* 1992;112(2-3):215-230.

15. Caravatti P, Allemann M. The ‘infinity cell’: A new trapped-ion cell with radiofrequency covered trapping electrodes for fourier transform ion cyclotron resonance mass spectrometry. *Organic Mass Spectrometry.* 1991;26(5):514-518.
16. Gerretzen J, Szymanska E, Jansen JJ, et al. Simple and Effective Way for Data Preprocessing Selection Based on Design of Experiments. *Analytical chemistry.* 2015;87(24):12096-12103.
17. Eliasson M, Rannar S, Madsen R, et al. Strategy for optimizing LC-MS data processing in metabolomics: a design of experiments approach. *Analytical chemistry.* 2012;84(15):6869-6876.
18. Eriksson L. Design of Experiments: Principles and Applications

Umetrics. 2008.
19. Lemonakis N, Skaltsounis AL, Tsarbopoulos A, Gikas E. Optimization of parameters affecting signal intensity in an LTQ-orbitrap in negative ion mode: A design of experiments approach. *Talanta.* 2016;147:402-409.
20. Tebani A, Schmitz-Afonso I, Rutledge DN, Gonzalez BJ, Bekri S, Afonso C. Optimization of a liquid chromatography ion mobility-mass spectrometry method for untargeted metabolomics using experimental design and multivariate data analysis. *Analytica chimica acta.* 2016;913:55-62.
21. Khare BN, Sagnan C, Zumberge JE, Sklarew DS, Nagy B. Organic Solids Produced by Electrical Discharge in Reducing Atmospheres Tholin Molecular Analysis. *Icarus.* 1981;48:290-297.
22. Coll P, Coscia D, Smith N, et al. Experimantal laboratory simulation of Titan's atmosphere: aerosols and gas phase. *Planetary and Space Science.* 1999;47:1331-1340.
23. Somogyi A, Oh CH, Smith MA, Lunine JI. Organic environments on Saturn's moon, Titan: simulating chemical reactions and analyzing products by FT-ICR and ion-trap mass spectrometry. *Journal of the American Society for Mass Spectrometry.* 2005;16(6):850-859.
24. Szopa C, Cernogora G, Boufendi L, Correia JJ, Coll P. PAMPRE: A dusty plasma experiment for Titan's tholins production and study. *Planetary and Space Science.* 2006;54(4):394-404.
25. Imanaka H, Smith MA. Formation of nitrogenated organic aerosols in the Titan upper atmosphere. *Proceedings of the National Academy of Sciences.* 2010;107.
26. Maillard J, Carrasco N, Schmitz-Afonso I, Gautier T, Afonso C. Comparison of soluble and insoluble organic matter in analogues of Titan's aerosols. *Earth and Planetary Science Letters.* 2018;495:185-191.
27. Gautier T, Carrasco N, Buch A, Szopa C, Sciamma-O’Brien E, Cernogora G. Nitrile gas chemistry in Titan’s atmosphere. *Icarus.* 2011;213(2):625-635.
28. Barrere C, Hubert-Roux M, Lange CM, et al. Solvent-based and solvent-free characterization of low solubility and low molecular weight polyamides by mass spectrometry: a complementary approach. *Rapid communications in mass spectrometry : RCM.* 2012;26(11):1347-1354.
29. Montgomery D. Design and Analysis of Experiments. *John Wiley & Sons.* 2008.
30. Niemann HB, Atreya SK, Bauer SJ, et al. The abundances of constituents of Titan's atmosphere from the GCMS instrument on the Huygens probe. *Nature.* 2005;438(7069):779-784.
31. Fulchignoni M, Ferri F, Angrilli F, et al. In situ measurements of the physical characteristics of Titan's environment. *Nature.* 2005;438(7069):785-791.

435 32. Lebreton JP, Witasse O, Sollazzo C, et al. An overview of the descent and landing
436 of the Huygens probe on Titan. *Nature.* 2005;438(7069):758-764.
437 33. Israel G, Szopa C, Raulin F, et al. Complex organic matter in Titan's atmospheric
438 aerosols from in situ pyrolysis and analysis. *Nature.* 2005;438(7069):796-799.
439 34. Sagan C. The origin of life in a cosmic context. *Origins of Life.* 1974;5(3-4):497-
440 505.
441 35. Sagan C, Thompson WR, Khare BN. Titan: a laboratory for prebiological organic
442 chemistry. *Accounts of Chemical Research.* 2002;25(7):286-292.

443

444

7. Figure and tables

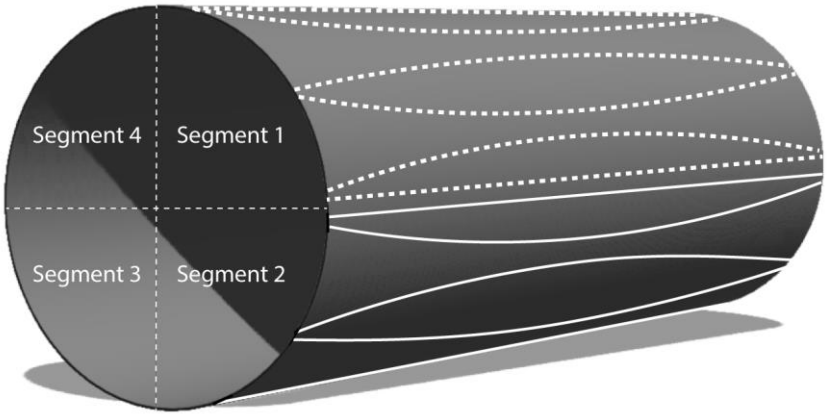

Figure 1: Schematic representation of a dynamically harmonized ICR cell. The cell is divided into four segments representing each adjustable parameter: Segment 1 (in dashed lines) is for shimming and gating 0°, segment 2 (in solid lines) for shimming and gating 90°, segment 3 for shimming and gating 180° and segment 4 for shimming and gating 270°.

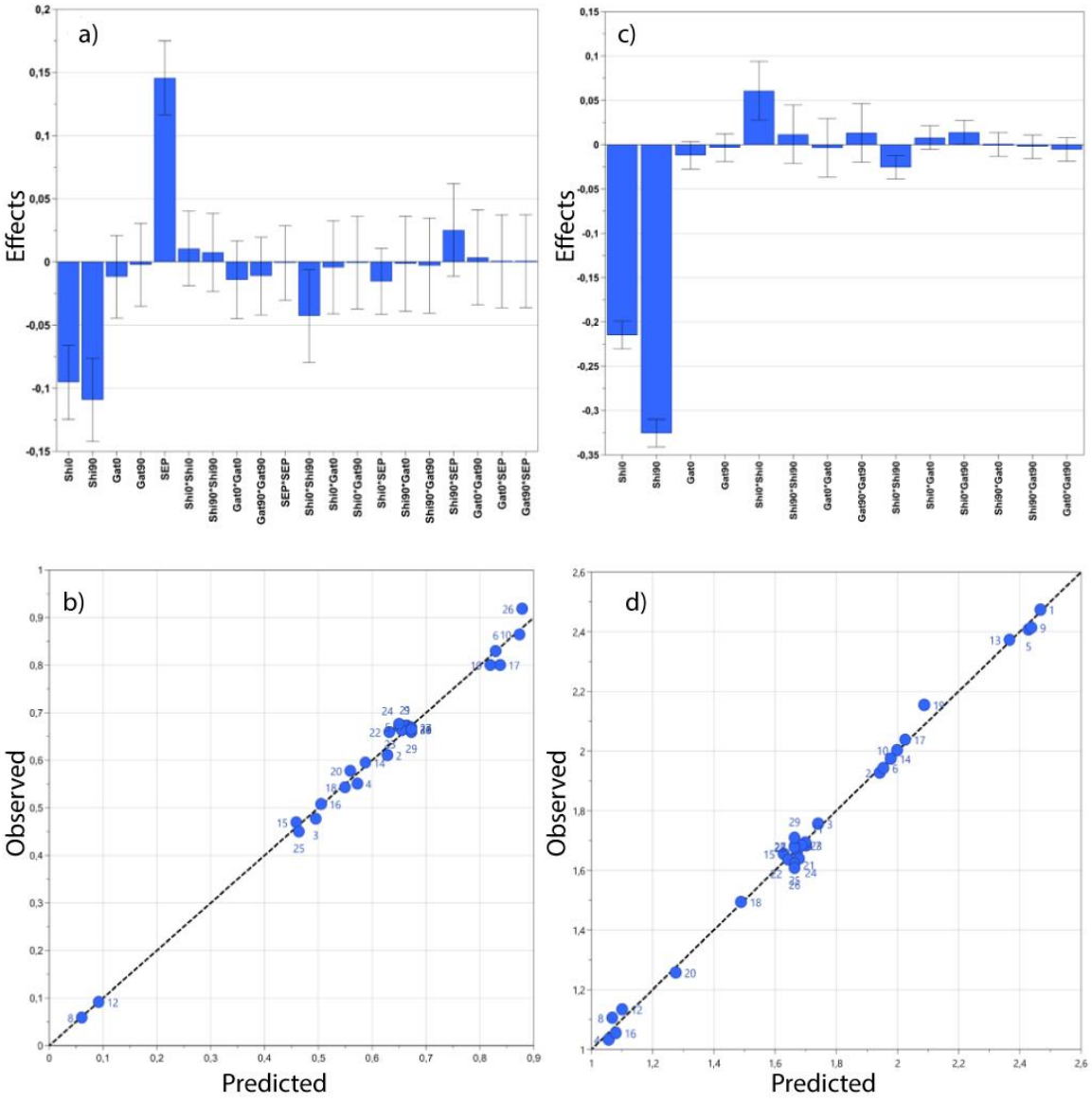

453

454 Figure 2: a) Observation of the effects of the different factors on the even harmonic
455 magnitude for the screening step, b) Prediction plot between the predicted and observed
456 values of the second harmonic magnitude for the screening step, c) Observation of the
457 effects of the different factors on the second harmonic magnitude for the optimization step,
458 d) Prediction plot between the predicted and observed values of the second harmonic
459 magnitude for the optimization step.
460

461

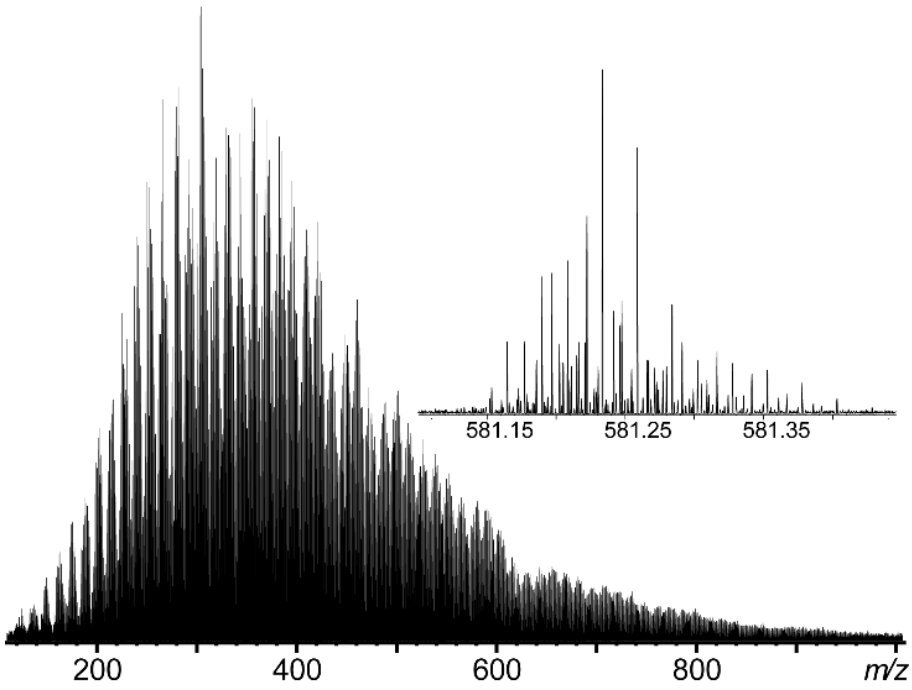

Figure 3: LDI spectrum in positive mode of a tholins sample obtained after deploying the cell parameter optimized with the DoE approach, revealing more than 50,000 peaks. The inset visualized a close zoom between *m/z* 581.15 and *m/z* 581.40 illustrating the high isobaric complexity.

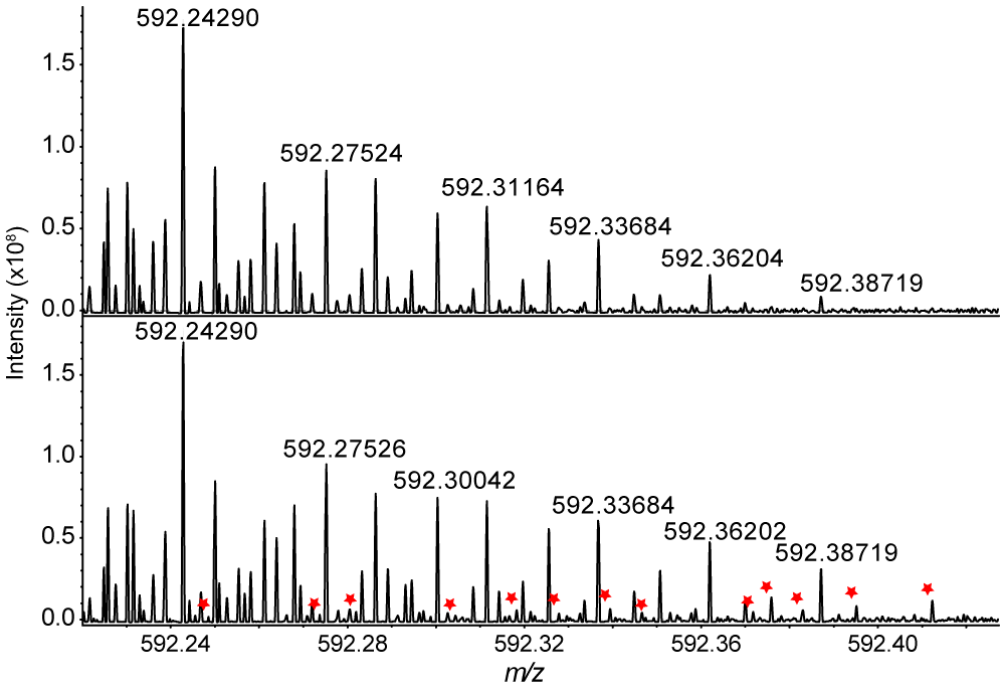

Figure 4: (Top) Zoom on the tholins spectrum obtained after a manual optimization (shimming) of the ICR cell parameters. (Bottom) Tholins spectrum obtained after applying the parameters given by the DoE optimization. Red dots indicate species found after DoE optimization and not detected after manual optimization.

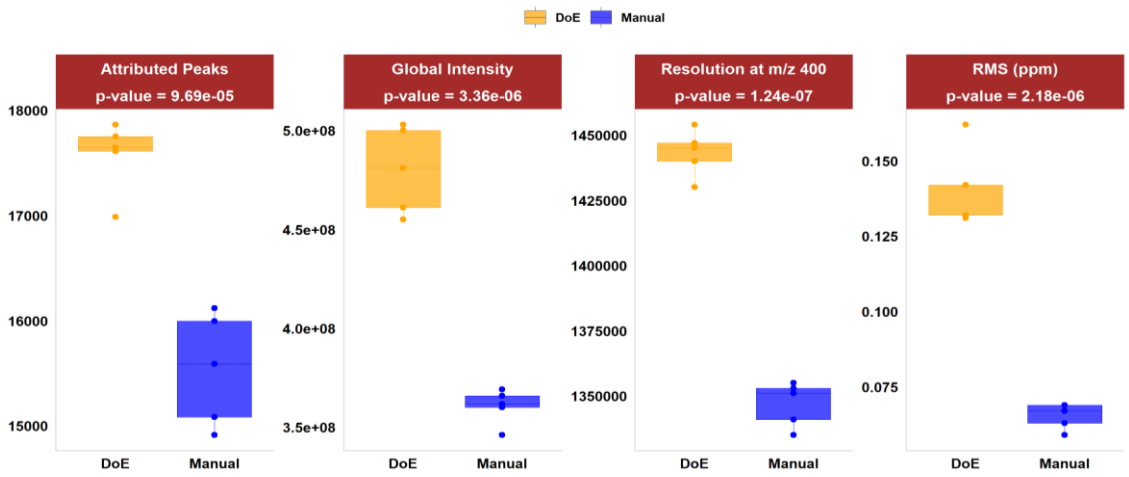

Figure 5: Comparison of attributed peaks, global intensity, resolution and RMS between the manually optimized spectrum and the DoE spectrum of a tholins sample.

Table 1: Coded composite face design (CCF) design matrix for experimental screening on NaTFA

Run N°	Run Order	Shi0	Shi90	Gat0	Gat90	SEP
1	10	-1	-1	-1	-1	1
2	28	1	-1	-1	-1	-1
3	23	-1	1	-1	-1	-1
4	9	1	1	-1	-1	1
5	1	-1	-1	1	-1	-1
6	24	1	-1	1	-1	1
7	20	-1	1	1	-1	1
8	12	1	1	1	-1	-1
9	29	-1	-1	-1	1	-1
10	8	1	-1	-1	1	1
11	6	-1	1	-1	1	1
12	5	1	1	-1	1	-1
13	25	-1	-1	1	1	1
14	16	1	-1	1	1	-1
15	26	-1	1	1	1	-1
16	17	1	1	1	1	1
17	2	-1	0	0	0	0
18	13	1	0	0	0	0
19	15	0	-1	0	0	0
20	19	0	1	0	0	0
21	4	0	0	-1	0	0
22	14	0	0	1	0	0
23	18	0	0	0	-1	0
24	22	0	0	0	1	0
25	3	0	0	0	0	-1
26	7	0	0	0	0	1
27	27	0	0	0	0	0
28	31	0	0	0	0	0
29	30	0	0	0	0	0
30	11	0	0	0	0	0
31	21	0	0	0	0	0

479

480

Table 2: Predicted values for each factor for the screening and optimization step

Screening step

Factor	Intervals	Predicted Value	Factor contribution (%)
Shim0	1.465 to 1.535 (V)	1.535V	15.4
Shim90	1.465 to 1.540 (V)	1.540V	33.3
Gat0	1.4 to 1.620 (V)	1.620V	12.6
Gat90	1.450 to 1.550 (V)	1.550V	10.7
Sweep	20 to 40 (%)	20%	28.0

Optimization step

Factor	Intervals	Predicted Value	Factor contribution (%)
Shim0	1.530 to 1.550 (V)	1.542V	53.1
Shim90	1.530 to 1.550 (V)	1.550V	43.4
Gat0	1.600 to 1.640 (V)	1.600V	1.9
Gat90	1.540 to 1.570 (V)	1.551V	1.7

Table 3. Comparison of the mass spectrometric response of the LDI tholins spectra deploying manufacturer default values (before tuning), conventional manual tuning (manual), and parameters given by the DoE optimization method. p-values refers to the comparison between manual Tuning and the DoE strategy. (p-value > 0.05 is considered as significant)

	DoE (Mean)	Manual (Mean)	p-value	Fold Change
Attributed Peaks	$1.76\ 10^{+04}$	$1.55\ 10^{+04}$	$9.69\ 10^{-05}$	1.13
Global Intensity	$4.80\ 10^{+08}$	$3.61\ 10^{+08}$	$3.36\ 10^{-06}$	1.33
Resolution at m/z 400	$1.44\ 10^{+06}$	$1.35\ 10^{+06}$	$1.24\ 10^{-07}$	1.07
RMS (ppm)	0.140	0.0654	$2.18\ 10^{-06}$	2.14

Supplementary Information for

Optimization of ion trajectories in a dynamically harmonized Fourier-Transform Ion Cyclotron Resonance cell using a Design of Experiments strategy

Julien MAILLARD[1,2], Justine FEREY[2], Christopher P. Rüger[2], Isabelle SCHMITZ-AFONSO[2], Soumeya BEKRI[3], Thomas GAUTIER[1], Nathalie CARRASCO[1], Carlos AFONSO[2] and Abdellah TEBANI[2,3*]

[1] LATMOS/IPSL, Université Versailles St Quentin, UPMC Université Paris 06, CNRS, 11 blvd d'Alembert, F-78280 Guyancourt, France

[2] Université de Rouen, Laboratoire COBRA UMR 6014 & FR 3038, IRCOF, 1 Rue Tesnière, 76821 Mont St Aignan Cedex, France

[3] Department of Metabolic Biochemistry, Rouen University Hospital, Rouen, 76000, France

This PDF file includes:

Tables S-1 to S-6

Captions:

- **Table S-1:** Fractional Factorial design matrix with response values for the screening step.
- **Table S-2:** Fractional Factorial design matrix with response values for the optimization step.
- **Table S-3:** PLS model regression coefficients generated by the screening step.
- **Table S-4:** ANOVA test results of the PLS model generated by the screening step.
- **Table S-5:** PLS model regression coefficients generated by the optimization step.
- **Table S-6:** ANOVA test results of the PLS model generated by the optimization step.

Table S-1: Fractional Factorial design matrix with response values the screening step.

Run Nº	Run Order	Shim0 (V)	Shim90 (V)	Gat0 (V)	Gat90 (V)	SEP (%)	Second harmonic (%)
1	10	1.465	1.465	1.400	1.450	40	
2	28	1.535	1.465	1.400	1.450	20	4.083
3	23	1.465	1.540	1.400	1.450	20	2.996
4	9	1.535	1.540	1.400	1.450	40	3.558
5	1	1.465	1.465	1.620	1.450	20	4.694
6	24	1.535	1.465	1.620	1.450	40	6.77
7	20	1.465	1.540	1.620	1.450	40	
8	12	1.535	1.540	1.620	1.450	20	1.143
9	29	1.465	1.465	1.400	1.550	20	4.714
10	8	1.535	1.465	1.400	1.550	40	7.312
11	6	1.465	1.540	1.400	1.550	40	
12	5	1.535	1.540	1.400	1.550	20	1.237
13	25	1.465	1.465	1.620	1.550	40	
14	16	1.535	1.465	1.620	1.550	20	3.937
15	26	1.465	1.540	1.620	1.550	20	2.946
16	17	1.535	1.540	1.620	1.550	40	3.228
17	2	1.465	1.503	1.510	1.500	30	6.332
18	13	1.535	1.503	1.510	1.500	30	3.494
19	15	1.500	1.465	1.510	1.500	30	6.305
20	19	1.500	1.540	1.510	1.500	30	3.788
21	4	1.500	1.503	1.400	1.500	30	4.716
22	14	1.500	1.503	1.620	1.500	30	4.56
23	18	1.500	1.503	1.510	1.450	30	4.599
24	22	1.500	1.503	1.510	1.550	30	4.747
25	3	1.500	1.503	1.510	1.500	20	2.819
26	7	1.500	1.503	1.510	1.500	40	8.281
27	27	1.500	1.503	1.510	1.500	30	4.659
28	31	1.500	1.503	1.510	1.500	30	4.627
29	30	1.500	1.503	1.510	1.500	30	4.567
30	11	1.500	1.503	1.510	1.500	30	4.629
31	21	1.500	1.503	1.510	1.500	30	4.624

527

528

Table S-2: Fractional Factorial design matrix with response values for the optimization step.

Run N°	Run Order	Shim0 (V)	Shim90 (V)	Gat0 (V)	Gat90 (V)	Second harmonic (%)
1	27	1.530	1.530	1.600	1.540	2.475
2	2	1.550	1.530	1.600	1.540	1.928
3	20	1.530	1.550	1.600	1.540	1.757
4	4	1.550	1.550	1.600	1.540	1.033
5	5	1.530	1.530	1.640	1.540	2.407
6	23	1.550	1.530	1.640	1.540	1.942
7	12	1.530	1.550	1.640	1.540	1.684
8	24	1.550	1.550	1.640	1.540	1.107
9	19	1.530	1.530	1.600	1.570	2.414
10	6	1.550	1.530	1.600	1.570	2.003
11	26	1.530	1.550	1.600	1.570	1.693
12	3	1.550	1.550	1.600	1.570	1.135
13	1	1.530	1.530	1.640	1.570	2.373
14	11	1.550	1.530	1.640	1.570	1.975
15	28	1.530	1.550	1.640	1.570	1.654
16	29	1.550	1.550	1.640	1.570	1.054
17	17	1.530	1.540	1.620	1.555	2.039
18	18	1.550	1.540	1.620	1.555	1.493
19	8	1.540	1.530	1.620	1.555	2.156
20	10	1.540	1.550	1.620	1.555	1.256
21	21	1.540	1.540	1.600	1.555	1.665
22	22	1.540	1.540	1.640	1.555	1.637
23	16	1.540	1.540	1.620	1.540	1.684
24	15	1.540	1.540	1.620	1.570	1.639
25	25	1.540	1.540	1.620	1.555	1.623
26	14	1.540	1.540	1.620	1.555	1.608
27	13	1.540	1.540	1.620	1.555	1.682
28	7	1.540	1.540	1.620	1.555	1.676
29	9	1.540	1.540	1.620	1.555	1.708

529

Table S-3: PLS model regression coefficients generated by the screening step.

Second harmonic

	Coeff. SC	Std. Err.	P
Shim0	-0.08870	0.01303	0.00049
Shim90	-0.11241	0.01455	0.00025
Gat0	-0.00704	0.01455	0.64563
Gat90	0.00193	0.01455	0.89872
SEP	0.14123	0.01303	0.00004
Shi0*Shi0	-0.00072	0.01310	0.95773
Shi90*Shi90	0.00442	0.01369	0.75791
Gat0*Gat0	-0.01040	0.01368	0.47577
Gat90*Gat90	-0.00789	0.01368	0.58525
SEP*SEP	0.00569	0.01310	0.67912
Shi0*Shi90	-0.04575	0.01633	0.03106
Shi0*Gat0	-0.00388	0.01633	0.81987
Shi0*Gat90	-0.00052	0.01633	0.97560
Shi0*SEP	-0.01725	0.01162	0.18826
Shi90*Gat0	-0.00212	0.01669	0.90321
Shi90*Gat90	-0.00107	0.01669	0.95099
Shi90*SEP	0.03057	0.01633	0.11029
Gat0*Gat90	0.00019	0.01668	0.99123
Gat0*SEP	-0.00032	0.01633	0.98493
Gat90*SEP	0.00031	0.01633	0.98555

N = 27	Q2 =	0.628	
DF = 6	R2 =	0.991	RSD = 0.03919
Comp. = 4	R2 adj. =	0.959	
			Confidence = 0.95

Table S-4: ANOVA test results of the PLS model generated by the screening step.

Second harmonic

	DF	SS	MS (variance)	F	p
Total	27	11.0417	0.40895		
Total corrected	26	0.972344	0.0373979		
Regression	20	0.96313	0.0481565	31.3577	**0**
Residual	6	0.00921428	0.00153571		

N = 27	Q2 =	0.628	Cond. no. = 12.05
DF = 6	R2 =	0.991	RSD = 0.03919
Comp. = 4	R2 adj. =	0.959	

Table S-5: PLS model regression coefficients generated by the optimization step.

Second harmonic

	Coeff. SC	Std. Err.	P
Constant	1,66208	0,0126069	4,58E-23
Shim0	-0,214759	0,0072904	5,37E-14
Shim90	-0,325479	0,00729039	1,69E-16
Gat0	-0,0120755	0,0072904	0,119882
Gat90	-0,00339587	0,0072904	0,648523
Shi0*Shi0	0,0608795	0,0154223	0,00145892
Shi90*Shi90	0,0117455	0,0154223	0,458943
Gat0*Gat0	-0,00371134	0,0154223	0,813317
Gat90*Gat90	0,0132228	0,0154223	0,405672
Shi0*Shi90	-0,0255319	0,00619991	0,00104456
Shi0*Gat0	0,00798444	0,0061999	0,218685
Shi0*Gat90	0,0138399	0,0061999	0,0424476
Shi90*Gat0	0,000118387	0,0061999	0,985034
Shi90*Gat90	-0,0022854	0,0061999	0,717926
Gat0*Gat90	-0,00542158	0,0061999	0,39662

N = 29	Q2 =	0,889	
DF = 14	R2 =	0,995	RSD = 0,03858
Comp. = 5	R2 adj. =	0,991	
			Confidence = 0,95

Table S-6: ANOVA test results of the PLS model generated by the optimization step.

Second harmonic

	DF	SS	MS (variance)	F	p
Total	29	92,3573	3,18473		
Total corrected	28	4,41765	0,157773		
Regression	14	4,39681	0,314058	211,033	0
Residual	14	0,0208347	0,00148819		

N = 29	Q2 =	0,889	Cond. no. =	6,106
DF = 14	R2 =	0,995	RSD =	0,03858
Comp. = 5	R2 adj. =	0,991		

538 **Table S-7: Attribution of new peaks detected after the DoE optimization**

539

Measured *m/z*	Molecular formula	Err. (ppm)
592.24866	C25H30N13O5	0.13
592.27374	C26H32N13O3^18O	-0.04
592.28203	C27H35N10O5^13C	-0.05
592.31836	C38H38N7	-0.06
592.32791	C19H41N14O7^15N	-0.14
592.33949	C25H43N10O6^13C	0.03
592.34673	C19H43N14O7^13C	-0.01
592.37013	C33H43N10^13C	-0.11
592.37597	C26H47N10O5^13C	-0.12
592.38314	C30H46N11O2	-0.17
592.39528	C35H47N8^13C	-0.17
592.41238	C37H50N7	-0.11